Eur Biophys J
DOI 10.1007/s00249-010-0667-y

ORIGINAL PAPER

Two methods of temperature control for single-molecule measurements

Matthew A. B. Baker · Yuichi Inoue · Kuniaki Takeda · Akihiko Ishijima · Richard M. Berry

Received: 27 September 2010 / Revised: 3 December 2010 / Accepted: 23 December 2010

Abstract Modern single-molecule biophysical experiments require high numerical aperture oil-immersion objectives in close contact with the sample. We introduce two methods of high numerical aperture temperature control which can be implemented on any microscope: objective temperature control using a ring-shaped Peltier device, and stage temperature control using a fluid flow cooling chip in close thermal contact with the sample. We demonstrate the efficacy of each system by showing the change in speed with temperature of two molecular motors, the bacterial flagellar motor and skeletal muscle myosin.

Keywords Temperature · Single molecule · Microscopy · Bacterial flagellar motor · Myosin

Introduction

Heating a biological sample on a microscope is relatively easy, either macroscopically using ohmic heating in coiled wires (Dox and Roark 1917) or microscopically using localised heating from lasers (Mao et al.2005; Paster and Ryu 2008), but cooling requires placing a heat sink in close thermal contact with the sample. We describe two methods of rapid (±20°C in 2 min) temperature control that enable measurements during temperature transients on a microscope with a high magnification objective.

Our first method (Fig. 1) uses a water-moderated ring-shaped Peltier heat pump mounted on an objective collar with a proportional–integral–differential (PID) feedback circuit controlling the Peltier current in response to a thermistor sensor. The recent advent of inexpensive commercially available ring-shaped Peltier plates makes Peltier cooling of objectives a practical approach for microscope cooling. Others have demonstrated the advantages of objective cooling systems (Mao et al.2005; Lambert and Bajer 1977; Anson 1992; Rabin and Podbilewicz 2000), namely rapid heat exchange between sample and objective, a wide range of accessible temperatures, and, when using a sandwich of two objectives, high temperature stability throughout the sample. Our work extends objective temperature control with rapid electronically moderated PID feedback. We have demonstrated function over a range of temperatures, in contrast with Komarova et al. (2009) who used Peltier control only to stabilize a sample at 25°C. Our Peltier controller is capable of heating or cooling 20°C in approximately 2 min, down to a minimum of −1.6°C with ice water coolant, and could reach colder temperatures with a salt/ice or antifreeze coolant. Extreme and rapid heating and cooling is, in practice, limited by the power of the heat-pump and the ability of the objective to withstand large and sudden temperature stresses (Leake et al. 2004). We calibrated the objective collar system by observing melting of microscopic droplets of wax, a technique adapted from Berg and Turner (1993), which gives us accurate calibration of the temperature of the sample itself.

Our second method (Fig. 2) uses fluid flowing through a chip directly above the sample to control the temperature in the range 6–50°C. A variant of this fluid chip was recently

Electronic supplementary material The online version of this article (doi:10.1007/s00249-010-0667-y) contains supplementary material, which is available to authorized users.

M. A. B. Baker · R. M. Berry (✉)
Clarendon Laboratory, Oxford University,
Parks Rd, Oxford OX1 3DP, UK
e-mail: r.berry1@physics.ox.ac.uk

Y. Inoue · K. Takeda · A. Ishijima
Institute of Multidisciplinary Research for Advanced Materials,
Tohoku University, Sendai, Japan

Published online: 30 January 2011

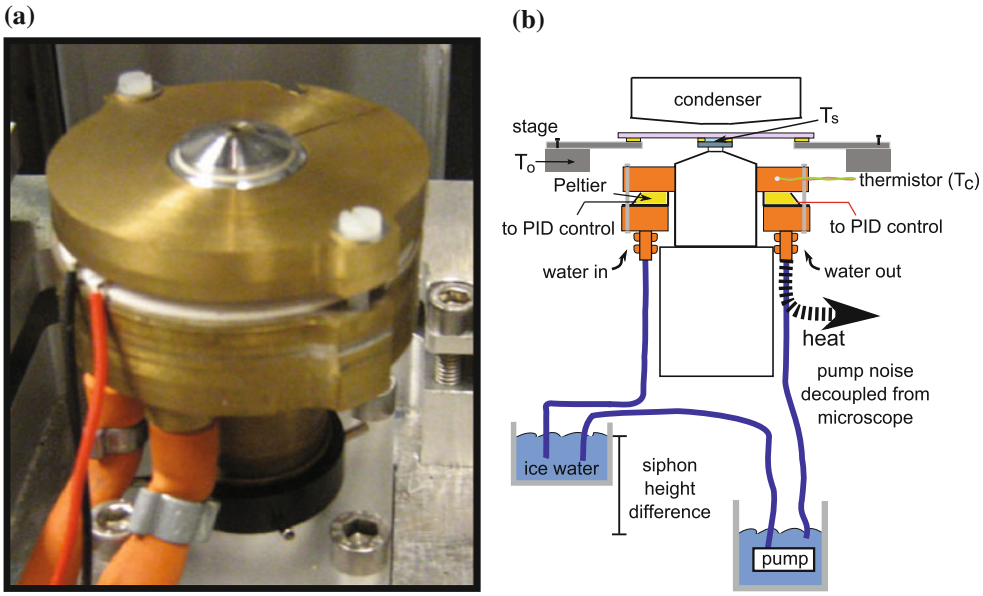

Fig. 1 The Peltier-cooled collar. **a** Image of the collar attached to the objective in place on the microscope. **b** Schematic diagram of the system, showing location of the thermistor to measure the temperature of the collar, which is correlated with sample temperature as shown in Fig. 3a. The bottom-side of the collar is regulated by water flow driven by gravity. The head of pressure for the siphon is maintained by pumping water back up to the higher reservoir which decouples the noise of the pump from the microscope and the stage

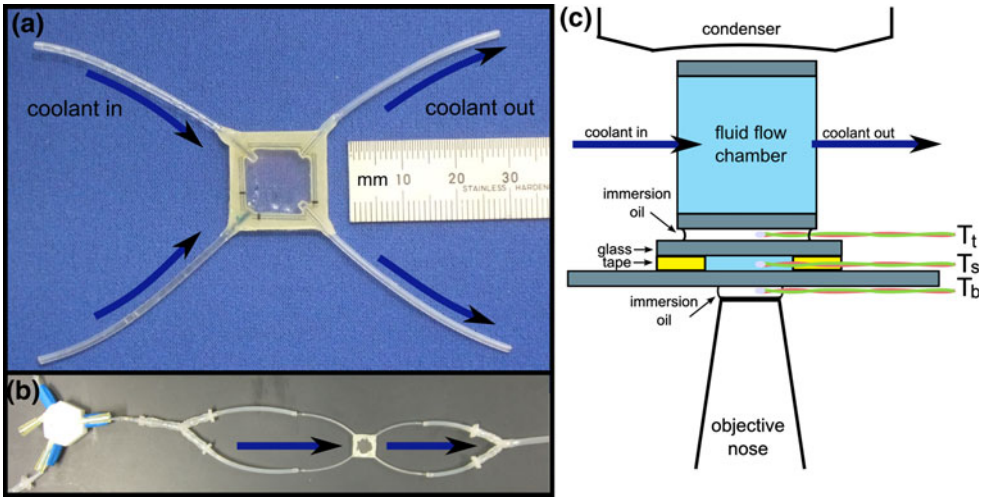

Fig. 2 **a** Top view of the fluid flow cooling chip. The fluid is pumped across the chip from the left side to the right side. **b** Fluid flow chip and switching gate. A switching gate switches flow from reservoirs of hot (70°C) or cold (−20°C) water, and fluid is split into two channels using Y-type connectors to make cooling more homogeneous across the chip. The chip cools or heats the sample by placing a large volume of water in close thermal contact with the sample. **c** Scale schematic diagram of the fluid chip temperature controller with 20:1 vertical:horizontal expansion. The three locations at which temperature was measured are indicated by the thermocouples (*top*: T_t; sample: T_s; *bottom* T_b). Two of these are measured simultaneously to determine sample temperature from the relationship shown in Fig. 3b

used to control the temperature on a low NA objective to measure thermotaxis in *E. coli* (Nishiyama et al. 2010), and here we extend its use to high-resolution microscopy.

We used these temperature controllers to observe two different molecular motors: the bacterial flagellar motor (BFM), the rotary motor that powers bacterial motility (Sowa and Berry 2008), and skeletal muscle myosin II, a linear motor that steps along actin filaments (Block 1996). Molecular motors are complexes that transduce chemical free energy into the mechanical work used for intracellular transport, cell division, or the motility of the entire cell (Baker and Berry 2009). The energy and kinetic cycles that convert chemical energy into force are affected by temperature change and the speed of a molecular motor is typically dependent on temperature. Single-molecule experiments with reversible and rapid temperature control have three primary advantages. First, there is a large reduction in the number of samples and trials that are necessary, because a single motor can be cycled through a range of temperatures. Second, measurements on a single motor can be verified by observing a reproducible response over multiple temperature cycles. Last, by studying single motors and their response to temperature, we can investigate short-lived changes in the motor state during heating

or cooling that would be lost to averaging in ensemble measurements.

Methods

Temperature control with the Peltier collar

The objective collar consists of two brass rings that sandwich a ring-shaped Peltier device (PE-032-14-15RH; Supercool, Sweden). The top section of the collar fits directly over the nose of the objective with its outer case removed. (Plan Fluor, 100×, N.A. = 1.30, Oil, Nikon). We used a custom-built microscope in which the objective was fixed relative to an air-table and focussing was achieved by moving the sample stage (for a commercial microscope care may be needed to lock the focus to prevent drift because of the extra weight of the collar). The collar is coated with thermal grease and tightened around the nose to ensure full thermal contact. The Peltier is attached to the underside of the top ring, the bottom ring completes the stack and is not in contact with the objective. The active side of the Peltier is thus in thermal contact with the objective, and can be used to heat or cool the objective, whereas the bottom ring circulates water either to cool the hot-side of the Peltier, when the collar is being used to cool the objective, or to heat the cold-side of the Peltier when the collar is being used to heat the objective. To ensure reproducibility we used a constant, measured, volume of immersion oil 10 µl. Water flow ($\sim$500 ml/min) is driven by siphon flow under gravity and the head of pressure is maintained by pumping water back to the higher level. This decouples from the microscope and stage the noise of the pump (MC-450; Micro-Jet, UK). Water at room temperature was used as coolant for the Peltier when both heating and cooling, with ice water at 0°C used when only cooling was desired.

A thermal insulation collar (Bioptech, US), which allowed dry nitrogen to be passed into a sealed space directly behind the objective to prevent water condensation, was found to be unnecessary. We believe this was because the cold collar and coolant piping reduced the humidity of the air close to the objective, such that the back of the objective remained above the dew point. Water condensation in the immersion oil on the nose of the objective occurred only if the objective was left uncovered.

Temperature measurement with the Peltier collar

The temperature is measured at two points: at the top of the collar (T_c) using a thermistor (TS136-170; Oven Industries, US) embedded in the top plate of the collar, and at the focal position within the sample (T_s) using a wax of known melting point. The wax technique from Berg and Turner (1993) was adapted and a range of waxes with melting points from 5.5 to 49.5°C were used. For temperatures above room temperature, the surface of a coverslip is coated in sonicated micron-sized particles of wax, which appear smooth and spherical when liquid, or jagged and polygonal when solid, indicating sample temperature on the surface. For temperatures below room temperature, the phase change of a liquid micron sized droplet to a solid micron-size particle is less noticeable. Instead the entire chamber is filled with wax and the phase transition is noted directly above the marked surface of the coverslip.

Six waxes with different melting points were used to calibrate the relationship between the thermocouple and the inside of the coverslip: tetradecane (5.5°C), cyclohexane (7.0°C), pentadecane (9.8°C), hexadecane (18.0°C), eicosane (36.7°C) and tetracosane (49.5°C) (Acros Organics, UK). An additional calibration point is the equivalence of the sample and collar at room temperature in the absence of temperature control ($T_s = T_c = 22$°C).

Feedback for the Peltier collar

Power is supplied to the Peltier device from a PID temperature controller (5C7-195; Oven Industries), at a maximum of 4.0 A and 6.5 V. The unit measures the temperature at the collar using a thermistor (TS136-170; Oven Industries), and moderates the current supplied to the Peltier with a Ziegler-Nichols tuned PID response to drive temperature change quickly while minimising oscillation (Ziegler and Nichols 1993).

Temperature control with the fluid chip

The fluid chip method consists of a small chamber in close thermal contact with the sample carrying flowing fluid from a reservoir held at a fixed temperature, as shown in Fig. 2. The chamber is constructed from two coverslips (18 × 18 × 0.12–0.17 mm; Matsunami, Japan) with four glass pipettes used as spacers to create a chamber that is 18 × 18 × 1 mm. At the four corners of the chamber four polyethylene tubes are connected and the entire chamber is sealed using epoxy resin. The polyethylene tubes are then linked to tubing which has an external diameter of 3 mm and an internal diameter of 1 mm, and these are assembled using connectors (Y-type VFY306; Isis, Japan) in the configuration shown in Fig. 2.

Ice water at the eutectic point with dissolved NaCl (23% *w*/*w*, −20°C), or hot water (70°C), is introduced into the water-cooling chip via the switching gate, shown on the left side of Fig. 2b. Sample temperature is controlled by the rate of flow (0.2–20 ml/min), which in turn is controlled by either a peristaltic pump (SJ-1220; Atto, Japan),

or the adjustable reservoir height using flow under gravity. The sample chamber consists of two coverslips attached to each other with double sided sticky-tape. Thermal contact between the chip and the sample is ensured by use of objective immersion oil, and likewise the sample is in thermal contact with the objective because of the layer of immersion oil coating the objective. Care was taken to use constant volumes of immersion oil. Water condensation was prevented by a flow of air over the fluid chip that had been dried by passage through a bottle containing dry silica gel.

Temperature measurement with the fluid chip

Using two thermocouple probes (ST-21E-010-TS1-ASP; Anritsu, Japan) temperature was measured simultaneously at two out of three locations:

1. at the immersion oil layer between the water-cooling chip and top of the sample chamber (T_t) ;
2. at the immersion oil layer between the sample and the objective (T_b); and
3. at the solution inside the sample chamber (T_s).

The area of contact between the objective and the coverslip was a circle of diameter ~ 6 mm. The temperatures measured by the thermocouple were found to be constant and reproducible within this circle. Therefore we expect negligible temperature variation across a field of view <200 μm within the sample plane.

Bacterial flagellar motor

Sample preparation

Experimental cultures of *E. coli* strain YS34 (Sowa et al. 2005) with plasmids pYS11 (sticky filament, chloramphenicol resistant) (Kuwajima 1988) and pYS13 (Na^+ powered chimera stators, PomAPotB, ampicillin resistant, IPTG induced) (Asai et al. 2003) were grown in 5 ml T-broth (1% Bacto tryptone Difco/85 mM sodium chloride) containing the appropriate antibiotics (25 μg/ml chloramphenicol, 50 μg/ml ampicillin) at 30°C. Inducer was present at low concentrations (5 μg/ml IPTG). Flagellar rotation measurements were performed in motility buffer consisting of 10 mM potassium phosphate, 0.1 mM EDTA, and 85 mM NaCl at pH 7.0. Cells had their filaments sheared using 26 G syringe needles (Sigma, UK) and were fixed to a glass coverslip (22×22 mm, Menzel-Gläser, Germany) in a tunnel slide (76×26 mm, Menzel-Gläser) prepared as described by Reid et al. (2006), and mounted on a custom-built perspex slide holder. The chamber was washed with dilute suspensions of polystyrene beads (Polysciences, US) in motility buffer (0.05–1.4% *w*/*w*. solid/water). Beads adhered through hydrophobic interactions to the sticky filament protein.

Speed and torque measurements

A weak 1,064 nm Nd:YAG laser (Elforlight, UK) was focussed on the bead. Bead motion was calculated by measuring the change in scattering because of bead displacement with a quadrant photo-diode in the back focal plane as described previously (Sowa et al. 2005).

Speeds were calculated from *x*–*y* traces of bead displacement by performing a 2-s running window Fourier transform and taking the highest peak of the power spectrum to determine the rotational velocity, ω. Microscope focus drift was approximately 50 μm in *z* for every 10°C. The bead was kept in focus by manually correcting the stage height using a piezo-controlled stage (controller: E-509.C3 and E-503, stage: PI-517.3CL; Physik Instrumente, Germany).

Speeds at stable temperatures were calculated by dividing sections of *x*–*y* data at steady temperature into segments of equal size and averaging power spectra over all segments. For 0.35 μm beads, the data at each steady temperature (either ~ 22 or ~ 13°C) were divided into segments of 0.1 s and the average power spectrum was calculated with corresponding speed resolution of 10 Hz. Gaussian peaks were fitted for the largest peak. For 0.75 μm beads, the *x*–*y* data at each steady temperature (5, 10, 22 and 30°C) were divided into segments of 1 s and the average power spectrum was calculated with corresponding speed resolution of 1 Hz. Up to two Gaussian peaks were fitted. Peaks below 5 Hz, corresponding to transiently stopped or partially rotating motors were ignored for Gaussian fitting. Averaged power spectra for the *x*–*y* data at stable temperature for the 0.35 and 0.75 μm bead, respectively, are shown in Figs. S1 and S2 in the Supporting Information.

Myosin

Sample preparation

Skeletal myosin and actin filaments were extracted from rabbit skeletal muscle and purified as described previously by Harada et al. (1990). Use of myosin in the form of myosin filaments, as described elsewhere (Saito et al. 1994), ensured that all actin filaments moved when ATP was added. The sample chamber coverslip glass was cleaned with 0.1 M KOH and ethanol, and then coated with 5% Sigmacote (058K4363; Sigma-Aldrich, Japan). The sample chamber of ~ 20 μl was made from the coated

glass (24 mm × 50 mm; Matsunami) and uncoated glass (22 mm × 26 mm, Matsunami) using double sided sticky-tape as spacers. 20 µl of myosin solution containing ~30 mg/ml myosin was introduced into the chamber and left to incubate for ~1 min. This was then washed twice in 120 mM buffer (120 mM KCl, 20 mM HEPES-KOH (pH 7.0), 5 mM $MgCl_2$) and a further two times in 25 mM buffer (25 mM KCl, 20 mM HEPES-KOH (pH 7.0), 5 mM $MgCl_2$). Then 20 µl of actin solution (0.1 µg/ml, actin filaments stabilized by tetramethylrhodamine-labelled phalloidin (Yanagida et al. 1984)) in the presence of a glucose–glucose-oxidase oxygen scavenging system was introduced and the mixture was incubated for 1 min (Harada et al. 1990). Finally 20 µl of 2 mM ATP was introduced and the chamber was sealed with nail varnish.

Measurement of velocity

The chamber was mounted on an inverted microscope (IX70; Olympus) with an oil immersion lens (Plan Apo, 100x, N.A. = 1.40, Oil; Olympus). Temperature was controlled with the fluid chip. Fluorescence of labelled actin filaments was imaged using a CCD camera (WAT-100N; Watec, Japan) via a video timer (VTG-33; Fora, Japan). Temperature was controlled by switching the temperature of the inlet fluid between −20 and 70°C. Video images were digitized and the velocity of actin filaments was analysed using software ImageJ (NIH, US). Myosin speeds were calculated over window lengths of 1 s (0–10 µm/s) or 0.33 s (10–20 µm/s). Data points are mean ± SD of 9–16 measurements taken at each temperature.

Results

Calibration

The linear relationship between the temperature of the collar and the sample is shown in Fig. 3a. During biophysical measurements the temperature of the collar (T_c) is used to estimate sample temperature (T_s) from the calibrated relationship derived from the linear fit,

$$T_s = (0.843 \pm 0.016) \times T_c + (3.8 \pm 0.5). \quad (1)$$

where all temperatures are in °C.

For the chip temperature controller the relationship between all three temperatures; T_s, T_t and T_b is shown in Fig. 3b. During biophysical measurements the temperature measured at the site above the sample (T_t) is used to estimate the sample temperature from the calibrated relationship (Eq. 2) derived from the linear fits,

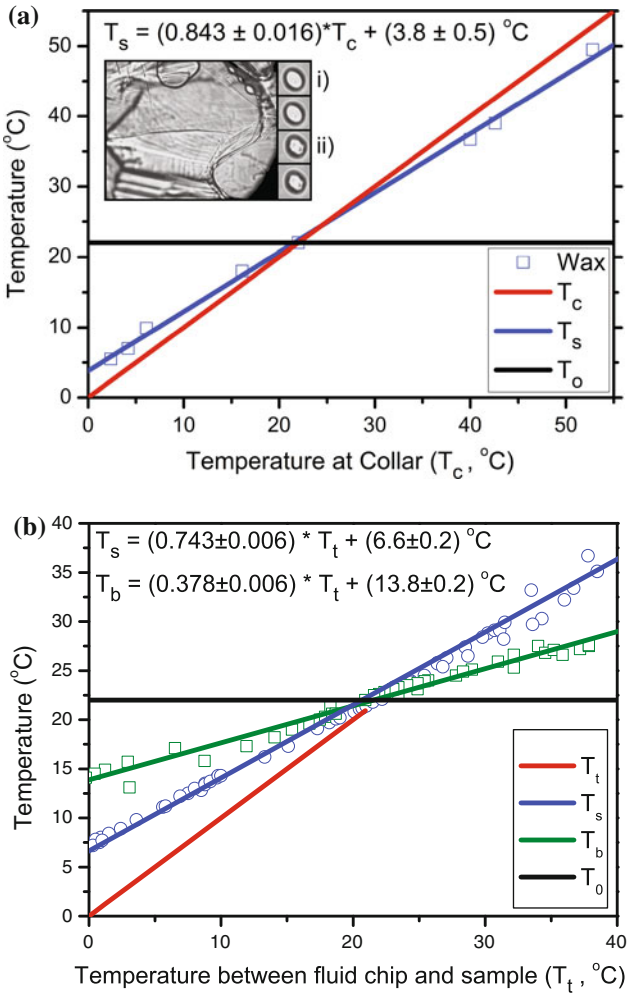

Fig. 3 **a** Linear relationship between the temperature measured at different locations for each temperature controller. **a** Relationship for collar between temperature as measured on the coverslip using waxes of known melting point and measured on the collar using a thermistor. The *inset* shows a chamber entirely full of wax during a phase transition from solid to liquid, and also (*i*) two spherical droplets in the liquid phase, (*ii*) two jagged crystals in the solid phase. Temperatures at the collar and at the sample were measured with a precision of ±0.1–0.2°C, and the error for the melting points of the waxes is ±0.1°C. The equivalence at room temperature ($T_0 = 22$°C) is added and used for fitting. **b** Linear temperature relationships between the three sites used to measure temperature for the chip temperature controller. The temperature was measured simultaneously by thermocouples at two out of three locations: T_t, between the chip and the sample (*red*), T_s, inside the sample (*blue*), and T_b between the sample and the objective (*green*). Temperatures from the thermocouple were measured with a precision of ±0.1°C. In both cases the steady-state room temperature ($T_0 = 22$°C) is indicated in *black*

$$T_s = (0.743 \pm 0.006) \times T_t + (6.7 \pm 0.2) \quad (2)$$

$$T_b = (0.378 \pm 0.006) \times T_t + (13.9 \pm 0.2) \quad (3)$$

where all temperatures are in °C.

The lower limit of sample temperature using coolant at −20°C was −6°C, but the typical temperature induced was 6–10°C. In practice T_s varied ±1°C between different runs at the same nominal flow rate restricting the ease with which the fluid chip can be set to a specific sample temperature.

Temperature response

Using the objective method, changing the temperature by 20°C to or from room temperature took 1–2 min depending on the previous history of temperature changes. For a sample equilibrated at room temperature (22°C), heating to 40°C and immediately cooling back to 22°C take 99 and 71 s, respectively (Fig. 4a). For a sample held at 40°C for >15 min and transiently cooled to 22°C, heating and cooling times are 46 and 93 s, respectively (Fig. 4b), the difference being because of the thermal inertia of the system. The time responses of the cooling chip were measured for flow rates that give sample temperatures of 40 and 8°C with fluid inlet temperatures of 70 and −20°C, respectively (Fig. 4c). Sample temperature during heating and cooling approached the steady-state value exponentially with time constants of ∼30 s. When flow was stopped, the sample temperature decayed exponentially back to room temperature with time constants of ∼50 s. Neither temperature controller adds significantly to the position detection noise of the system, with noise levels below 0.01 $nm^2\,Hz^{-1}$ at frequencies between 10 and 500 Hz (Fig. 5).

Motor response

Rotational speed of the BFM depends upon changes in temperature, with greater temperature dependence at low load than at high load (Berg and Turner 1993). Figure 6a–d

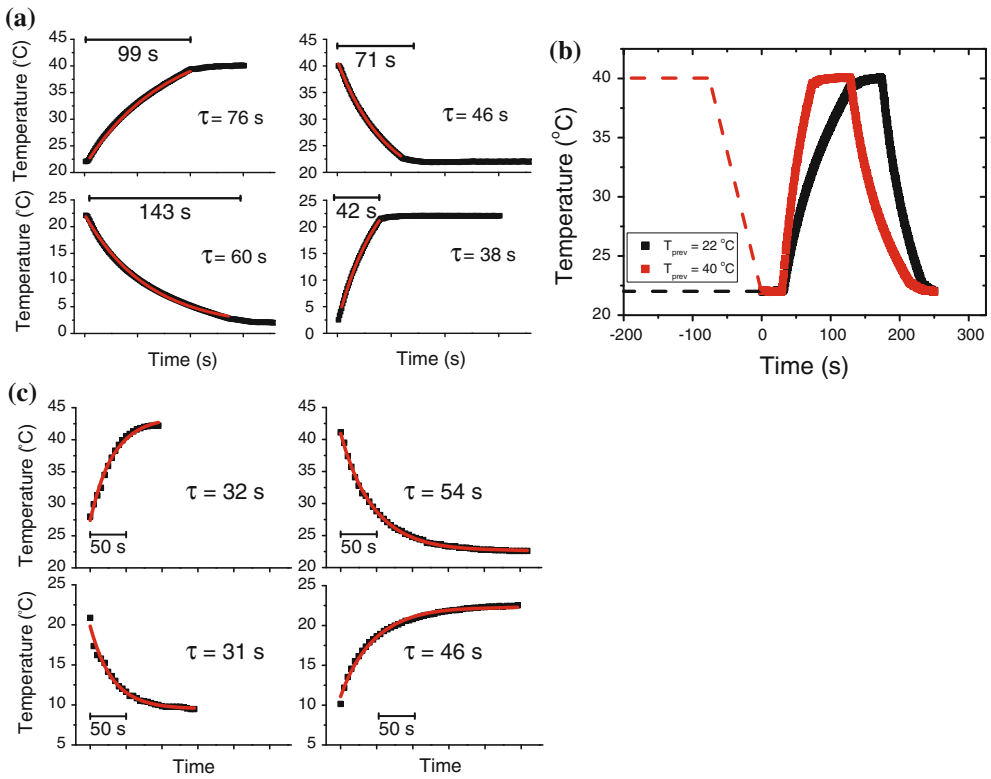

Fig. 4 Closer detail of temperature response for collar (**a**) and chip (**c**) with exponential fits and durations for temperature response with the microscope at equilibrium at 22°C and then driven to 40 or 2°C respectively, and then driven back to room temperature at 22°C. **a** Exponential fits are taken when the Peltier is being driven at maximum power, and represent the time constant for the exponential curve describing the long-term equilibrium temperature when the Peltier is run at full power. In practice, the PID controller reduces the power as the set point is approached, and so the duration of the change is also indicated as a measure of the controller's performance. Durations are measured as time taken to complete 95% of the temperature change. **b** Thermal inertia of the objective collar system. Overlaid temperature vs. time traces comparing a system previously at long term equilibrium at room temperature (22°C, *black squares*) with one that was held for 15 min at 40°C and then cooled to 22°C (*dashed line*) immediately before temperature recording (T_{prev} = 40°C, *red squares*). Temperature changes away from the previous long-term temperature are considerably slower than changes towards the previous long term temperature. **c** Time response of heating and cooling for the chip with exponential fits and time constants shown heating and cooling away from room temperature (*left*) and relaxation back to room temperature (*right*)

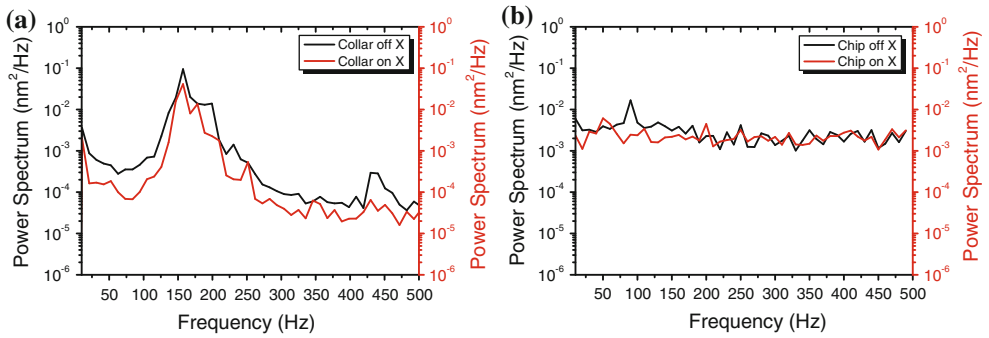

Fig. 5 Position detection noise profiles for the detector for each temperature controller. **a** Power spectrum of the *x*-position of a surface-bound bead with Peltier and gravity flow on (*red*), and off (*black*) for the Peltier collar controller. Data are sampled at 105 kHz, and the mean power spectrum is calculated over ten concurrent recordings of 0.1 s each. Data are shown only up to 500 Hz for comparison to the noise profile with the fluid chip. The slight increase in noise when cooling is off may be attributable to drainage of cooling water from the system. **b** Power spectrum of the *x*-position of a surface-bound bead with fluid chip flow on (*red*), and off (*black*). Data were sampled at a rate of 1 kHz and mean power spectrum calculated over ten concurrent recordings of 0.1 s duration each

shows changes in speed of 0.35 and 0.75 μm polystyrene microspheres attached to sodium-driven chimeric BFMs in *E. coli* (Sowa et al. 2005) during cycling of temperature, illustrating the capability of measuring speed during temperature transients using either the fluid chip or Peltier collar. The motor of Fig. 6a, b showed reproducible temperature-dependent speed changes between $\sim$12 and $\sim$20°C. The motor of Fig. 6c, d showed both reproducible and transient speed changes in response to temperature changes between 5 and 30°C. The sliding velocity of actin on a surface coated with myosin II (Fig. 6e, f) showed reproducible temperature-dependent speed changes in response to temperature changes between 6 and 38°C, consistent with previous work (Harada et al. 1990).

Discussion

Analysis of the thermal circuit

Both methods of temperature control work by pumping heat into or out of the sample; the fluid chip method through the stage it is mounted on, and the Peltier collar method through the objective underneath the sample. Heat flows in each system obey a linear relationship analogous to Ohm's Law for electrical currents, $Q = \Delta T/R$, where Q is the rate of heat flow through an element with thermal resistance R spanning a temperature difference ΔT. This relationship can be used to calculate the relative thermal resistances of different components of the system. Figure 7 displays a schematic and thermal circuit diagram for each system.

Efficacy of the Peltier collar method requires that the objective is in closer thermal contact with the sample than the sample is with the stage and surroundings ($R_s \gtrsim R_o$). With the surrounds at T_0 we may write:

$$T_s = T_0 + \frac{R_s}{R_s + R_o}(T_c - T_0) = T_0 + \alpha(T_c - T_0) \quad (4)$$

following from a direct analogy to an electrical potential divider, where $\alpha = R_s/(R_s + R_o)$. A linear fit to the blue line in Fig. 3a gives $\alpha = \frac{dT_s}{dT_c} = (0.843 \pm 0.016)$, indicating that $R_s/R_o = \alpha/(1-\alpha) = 5.37 \pm 0.14$.

For the fluid chip, the efficacy of the system depends on the thermal contact between the chip and the sample relative to that between the sample and the objective plus stage ($R_{os} \gtrsim R_1$). Similarly to Eq. 4, we may write:

$$T_s = T_0 + \frac{R_{os}}{R_1 + R_{os}}(T_t - T_0) = T_0 + \beta(T_t - T_0) \quad (5)$$

which, using a linear fit to the blue line in Fig. 3b, gives $\beta = \frac{dT_s}{dT_t} = 0.743 \pm 0.016$ and subsequently $R_{os}/R_1 = \beta/(1-\beta) = 2.89 \pm 0.03$.

Measurement of T_b (Fig. 3b) enables analysis of the thermal circuit of the fluid-flow chip if we assume that $R_s \gg (R_2 + R_3)$. Similarly to Eqs. 4 and 5 we may write:

$$T_s = T_b + \frac{R_1}{R_1 + R_2}(T_t - T_b) = T_b + \gamma(T_t - T_b) \quad (6)$$

$$= T_b(1-\gamma) + T_t\gamma. \quad (7)$$

Since $T_b = m_1 T_t + b_1$, where $m_1 = (0.378 \pm 0.006)$ and $b_1 = (13.9 \pm 0.2)$ °C, and $T_s = m_2 T_t + b_2$, where $m_2 = (0.743 \pm 0.006)$ and $b_2 = (6.7 \pm 0.2)$ °C (from linear fits in Fig. 3b), we have:

$$\frac{dT_s}{dT_t} = m_2 = m_1(1-\gamma) + \gamma \quad (8)$$

$$\Rightarrow \gamma = 0.587 \pm 0.010 \quad (9)$$

which gives $R_1/R_2 = \gamma/(1-\gamma) = 1.42 \pm 0.02$. Note that T_b differs substantially from T_0 (22°C) indicating substantial heat flow through the objective in the fluid chip

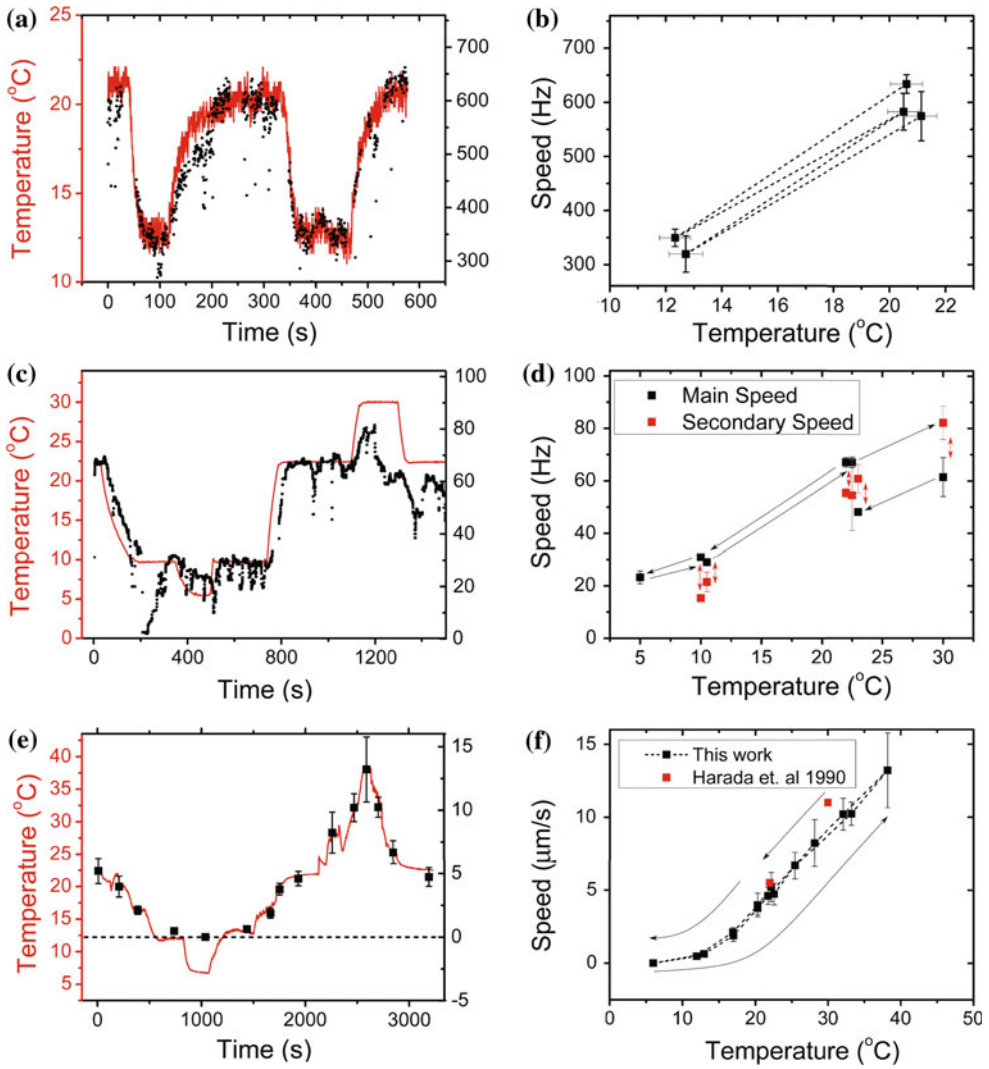

Fig. 6 Speed and temperature vs. time (*left*) and speed vs. temperature (*right*) for BFM rotation and actin filament sliding. **a**) Rotation of the BFM (*black circles*, 0.35 μm marker) and sample temperature (*red line*, fluid chip controlled) vs. time. **b** Speed vs. temperature for the data in (**a**). Over the range 12–22°C the speed of the BFM does not show hysteresis. **c** BFM rotation (*black circles*, 0.75 μm marker) and sample temperature (*red line*, Peltier collar controlled) vs. time. **d** Speed vs. temperature for the data shown in (*c*). Where more than one speed was observed at the same temperature, the main speed is shown in *black* and secondary speeds in *red*. The motor seems to jump between two or possibly three separate speed-temperature curves. **e** Actin sliding velocity (*black squares*) and temperature (*red line*, fluid chip controlled) vs. time. The speed of an actin filament across a surface coated in myosin motors slows to near stall at 12°C and increases to 13.2 μm/s at 40°C. **f** Actin speed (*black squares*) plotted as a function of temperature, using data from (**e**). The reproducibility of the cycle indicates no hysteresis over the range 6–40°C. *Arrows* in (**d**) and (**f**) indicate the approximate time-order of points in the speed-temperature plots

method. Also the large difference between T_t and the input temperature of the coolant (either 70 or −20°C) indicates temperature gradients in the coolant fluids which depend on flow rate, tubing insulation, and distance from the reservoir.

Conclusions

High speed temperature control provides a valuable tool to probe the kinetics and energetics of molecular motors and requires fast temperature controllers that do not impede optical sensitivity. We have demonstrated here two methods for controlling the temperature of a sample while retaining the nanometry necessary in single-molecule biophysical measurements. We designed objective-based and stage-based temperature controllers and characterized the corresponding thermal circuits. In the objective controller we found the thermal resistance between the sample and the environment was $\sim 5\times$ greater than that between the sample and the objective. For stage-based temperature control we introduced a fluid-flow chip with a thermal

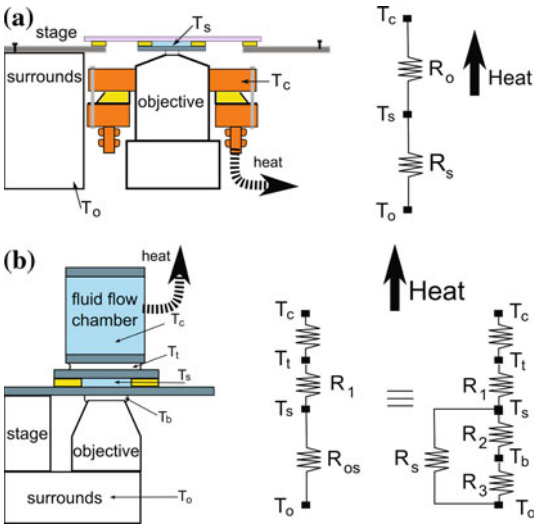

Fig. 7 **a** *Left*: Schematic diagram of the Peltier collar temperature controller in cooling mode. Heat flows into the sample from the surroundings (T_0) through the stage, which is in thermal contact with the surroundings. Heat flows out of the system through the Peltier device located in the collar, which acts as a heat pump pumping heat out of the system. *Right*. Thermal circuit for the Peltier collar. $R_s/R_o = 5.37 \pm 0.14$ is calculated as detailed in the text. **b** *Left*. schematic diagram of the fluid chip controller operating in cooling mode. Heat flows into the sample from the surroundings (T_0) through the stage and objective, which are in thermal contact with the sample. Heat flows out of the system through the cooling chip. The five locations shown in the circuit diagram are indicated. *Middle*. Reduced thermal circuit diagram for the fluid chip temperature controller. $R_{os}/R_1 = 2.89 \pm 0.03$ is calculated as detailed in the text. *Right*. The full circuit diagram including all measurement sites

resistance to the sample similar to that between the sample and the objective. Both methods are adaptable to different types of microscopes, and can change the temperature of a sample by ± 10°C in under a minute.

Our collar method is an improvement over fluid-cooled objective methods (Mao et al. 2005; Lambert and Bajer 1977; Anson 1992;Rabin and Podbilewicz 2000) primarily because it enables more rapid temperature changes. The most recent objective method (Mao et al. 2005) required 20 min to reach equilibrium at a new temperature, to a minimum of 4.5°C, with a drift of $\approx 2\,\mu$m/°C, whereas our controller can be used to measure temperature transients, down to a minimum of -1.6°C, but has a drift of $\approx 5\,\mu$m/°C. Mao et al. (2005) achieved high homogeneity (± 0.1°C throughout 2×2 mm) by using a sandwich of two objectives, one in place of a condenser, thus controlling the temperature from the top and bottom simultaneously (similar to Furuike et al. (2008)). This is useful for measurements in solution deep inside the sample chamber, and is a possible extension to our system; most single-molecule experiments are performed on or near the coverslip, however, and thus homogeneity in the z-direction is not critical.

The fluid chip method is ideal for making multiple measurements at an approximate fixed temperature, but is less suitable for making measurements at a range of specified temperatures, because that requires altering the fluid reservoir temperature or flow rate. Precise control ± 1°C is difficult to achieve because of varied heat loss from the tubing from the reservoir to the chip. The chip itself may be easily broken if roughly handled. These disadvantages are offset, however, by the low cost (only glass slides, tubing, and bottles are required), fast response, and ease of implementation.

Heat can also be applied more rapidly using lasers. Kato et al. (1999) used an IR laser to cause rapid local heating of metal aggregates (~ 20°C in ~ 20 m/s). This, however, caused a high temperature gradient 2°C/μm which restricted the precision of local temperature measurement. Mao et al. (2005) also experimented with using a 975 nm laser to cause a 5°C temperature rise in water molecules at the laser focus. They calculated that convection speeds would be 7 μm/s in a 90 μm/s chamber if a 27°C heat change was applied with a more powerful laser at an alternative wavelength and thus they did not combine their laser heating method with their cooling collar. Both of our methods could be extended to enable more rapid heating by incorporating a laser heating method. However, care would need to be taken to ensure that any improvement in heating speed was not offset by novel problems caused by convection or drift.

References

Anson M (1992) Temperature dependence and Arrhenius activation energy of F-actin velocity generated in *in vitro* by skeletal myosin. J Mol Biol 224:1029–38

Asai Y, Yakushi T, Kawagishi I, Homma M (2003) Ion-coupling determinants of Na^+-driven and H^+-driven flagellar motors. J Mol Biol 327:453–463

Baker MAB, Berry RM (2009) An introduction to the physics of the bacterial flagellar motor: a nanoscale rotary electric motor. Contemporary Phys 50:617–632

Berg H, Turner L (1993) Torque generated by the flagellar motor of *Escherichia coli*. Biophys J 65:2201–2216

Block SM (1996) Fifty ways to love your lever: myosin motors. Cell Mol Bioeng 87:151–7

Dox AW, Roark GW Jr (1917) The determination of gelatinization temperatures of starches by means of an electrically heated chamber on the microscope stage. J Am Chem Soc 39:742–745

Furuike S, Adachi K, Sakaki N, Shimo-Kon R, Itoh H, Muneyuki E, Yoshida M, Kinosita K (2008) Temperature dependence of the rotation and hydrolysis activities of F_1-ATPase. Biophys J 95:761–70

Harada Y, Sakurada K, Aoki T, Thomas DD, Yanagida T (1990) Mechanochemical coupling in actomyosin energy transduction studied by in vitro movement assay. J Mol Biol 216:49–68

Kato H, Nishizaka T, Iga T, Kinosita K, Ishiwata S (1999) Imaging of thermal activation of actomyosin motors. Proc Natl Acad Sci USA 96:9602–6

Komarova Y, Groot COD, Grigoriev I, Gouveia SM, Munteanu EL, Schober JM, Honappa S, Buey R, Hoogenraad C, Dogterom M (2009) Mammalian end binding proteins control persistent microtubule growth. J Cell Biol 184:691–706

Kuwajima G (1988) Construction of a minimum-size functional flagellin of *Escherichia coli*. J Bacteriol 170:3305–9

Lambert AM, Bajer AS (1977) Microtubules distribution and reversible arrest of chromosome movements induced by tow temperature. Cytobiologie 15:1–23

Leake MC, Wilson D, Gautel M, Simmons RM (2004) The elasticity of single titin molecules using a two-bead optical tweezers assay. Biophys J 87:1112–35

Mao H, Arias-Gonzalez JR, Smith SB, Jr IT, Bustamante C (2005) Temperature control methods in a laser tweezers system. Biophys J 89:1308–1316

Nishiyama S, Ohno S, Ohta N, Inoue Y (2010) Thermosensing function of the *Escherichia coli* Redox Sensor Aer. J Bacteriol 192:1740–1743

Paster E, Ryu W (2008) The thermal impulse response of *Escherichia coli*. Proc Natl Acad Sci USA 105:5373–5377

Rabin Y, Podbilewicz B (2000) Temperature-controlled microscopy for imaging living cells: apparatus, thermal analysis and temperature dependency of embryonic elongation in *Caenorhabditis elegans*. J Microsc 199:214–223

Reid SW, Leake MC, Chandler JH, Lo C-J, Armitage JP, Berry RM (2006) The maximum number of torque-generating units in the flagellar motor of *Escherichia coli* is at least 11. Proc Natl Acad Sci USA 103:8066–8071

Saito K, Aoki T, Aoki T, Yanagida T (1994) Movement of single myosin filaments and myosin step size on an actin filament suspended in solution by a laser trap. Biophys J 66:769–777

Sowa Y, Rowe AD, Leake MC, Yakushi T, Homma M, Ishijima A, Berry RM (2005) Direct observation of steps in rotation of the bacterial flagellar motor. Nat Biotechnol 437:916–919

Sowa Y, Berry RM (2008) Bacterial flagellar motor. Quart Rev Biophys 41:1–30

Yanagida T, Nakase M, Nishiyama K, Oosawa F (1984) Direct observation of motion of single F-actin filaments in the presence of myosins. Nat Biotechnol 207:58–60

Ziegler J, Nichols N (1993) Optimum settings for automatic controllers. J Dyn Syst 115:220–222